Mixed-Mode Fracture-Mechanics and Crack-Growth Analysis in Steam-Turbine Discs for Remaining-Life Assessment under Thermal Stresses and Mechanical Loading

Mohammad Farahi[1], Arina Agharafiee [1], Amir Mahdi Ebrahimi[1] and Omid Ashkani[2,*]

[1]Department of Mechanical Engineering, SR.C.IAU, Islamic Azad University, Tehran, Iran

[2]Department of Materials Engineering, SR.C.IAU, Islamic Azad University, Tehran, Iran

Abstract: The long-term performance and structural integrity of steam-turbine discs are strongly influenced by crack-growth behavior under combined thermal stresses and mechanical loading. In this study, a comprehensive analytical framework based on finite element analysis (FEA), mixed-mode fracture-mechanics evaluation (Modes I, II, and III), and fatigue crack-growth modeling using the Paris law is presented. The results indicate that Mode II plays the dominant role in the stress-intensity distribution and crack-growth behavior of the investigated turbine disc, while Modes I and III also contribute and cannot be neglected. Therefore, safety assessment based solely on Mode I analysis may lead to inaccurate evaluations of structural integrity. The calculated effective stress-intensity factor was compared with the fracture toughness of 12Cr steel, showing that the turbine disc currently operates within a safe margin against instantaneous fracture; however, gradual fatigue crack growth under thermo-mechanical loading conditions remains possible. The crack-growth analysis further demonstrates that a significant portion of the fatigue life is spent during the stable slow-growth phase as the crack propagates from small initial sizes to intermediate lengths. The proposed fracture-mechanics-based approach provides a reliable tool for condition monitoring, inspection planning, and remaining-life assessment of steam-turbine discs, thereby contributing to improved operational safety and maintenance decision-making.

Keywords: Fracture mechanics, Crack growth, Turbine, Finite element method (FEM), Heat transfer.

INTRODUCTION

At the beginning of the twentieth century, catastrophic failures in engineered structures revealed the limitations of traditional design approaches based solely on allowable stress criteria. In many cases, structures were observed to fail suddenly even when the applied stresses were lower than the yield strength of the material. This phenomenon directed researchers' attention toward the presence of micro-defects and discontinuities within materials, such as cracks. As a result, the field of fracture mechanics was developed to study the behavior of materials and structures containing cracks and defects. Within this framework, concepts such as the stress intensity factor, fracture energy, and fracture toughness were introduced to enable a more accurate and realistic analysis of material failure behavior [1, 2].

One of the fundamental topics in fracture mechanics is crack propagation, which refers to the gradual increase in the length of existing cracks within a material under static or cyclic loading conditions. Cracks may originate from manufacturing defects, residual stresses, corrosion processes, fatigue loading, or unfavorable operating conditions in engineering components. These initial cracks are often extremely small and may remain undetected during early stages of operation. However, under repeated loading they can progressively grow and eventually lead to sudden and catastrophic structural failure. For this reason, the study of crack growth is of great importance, as it enables the prediction of the remaining life of structural components and helps prevent unexpected failures. Crack growth analysis plays a crucial role not only in the safe design of structures but also in inspection planning, maintenance management, and improving the overall reliability of engineering systems [3, 6]. Figure **1** shows Comparison between the traditional mechanics method and the fracture mechanics method in structural integrity assessment.

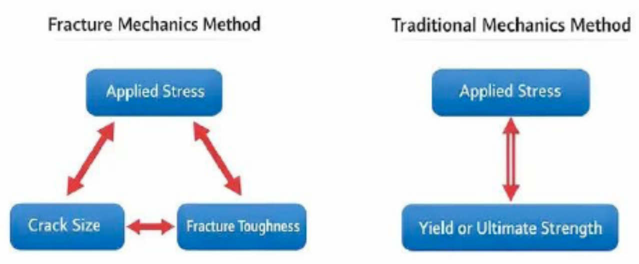

Figure 1: Comparison between the traditional mechanics method and the fracture mechanics method in structural integrity assessment.

Among various industrial sectors, the power generation industry is one in which equipment reliability and operational safety are of paramount importance. Steam power plants remain one of the major sources of electricity generation in many countries and contribute

*Address correspondence to this author at the Department of Materials Engineering, SR.C.IAU, Islamic Azad University, Tehran, Iran; E-mail: Omid.ashkani@srbiau.ac.ir; O.ashkani.14@gmail.com

Received on 01-08-2026 Accepted on 02-09-2026 Published on 03-09-2026

E-ISSN: 2409-9848/26

significantly to the stable supply of power within electrical grids. In these plants, thermal energy produced from the combustion of fossil fuels, nuclear reactions, or other heat sources is used to generate high-pressure and high-temperature steam. Through thermodynamic cycles, this thermal energy is converted into mechanical energy and ultimately into electrical power. Therefore, the reliable and continuous operation of steam power plants plays a critical role in maintaining grid stability, meeting electricity demand, and ensuring the secure operation of energy systems [7].

Within a steam power plant, the steam turbine is one of the most critical and sensitive components. It functions as the primary device responsible for converting the thermal energy of superheated steam into rotational mechanical energy. The mechanical energy generated by the turbine is then transmitted to a generator, where it is converted into electrical power and supplied to the grid. Any malfunction or structural damage in the main components of the turbine may lead to reduced plant efficiency, interruption of electricity generation, and potentially significant economic losses. Consequently, evaluating the mechanical integrity of turbine components and ensuring their safe operation are essential aspects of reliable and economical power plant operation [8, 9].

Figure 2: Schematic representation of a steam turbine rotor and disc assembly, illustrating the main structural components where stress concentration and crack initiation may occur.

Figure **2** and **3** shows a schematic of steam turbine. One of the key structural elements of steam turbines is the turbine disc, on which the blades are mounted and through which mechanical power is transmitted. During operation, these discs are subjected to extremely severe service conditions. In power plants operating with a grid frequency of 50 Hz, the turbine rotor typically rotates at approximately 3000 revolutions per minute. Under such conditions, turbine discs experience very high centrifugal stresses. In addition, elevated temperatures, strong thermal gradients, stresses associated with start-up and shutdown cycles, and dynamic loading conditions create complex stress fields within these components. Over time, these factors may contribute to the initiation of material defects or cracks in turbine discs. If such cracks grow progressively, they may eventually lead to critical failures [10, 11].

Since the sudden failure of turbine discs can have serious consequences for power plant safety and equipment integrity, evaluating crack behavior and predicting crack growth in these components are of great importance. Fracture mechanics provides an effective framework for analyzing stress conditions in the vicinity of crack tips and for assessing crack propagation behavior. By employing fracture mechanics parameters, particularly the stress intensity factor, it becomes possible to analyze crack behavior under different loading conditions and estimate the remaining service life of cracked components. Such analyses assist engineers in making informed decisions regarding plant operation, inspection intervals, and maintenance strategies [12, 14].

In the present study, crack growth in a steam turbine disc is investigated. This work represents a technical report based on real operational data obtained from a steam turbine in which a crack has been identified in one of the turbine discs. The primary objective of this study is to analyze crack behavior and estimate the remaining life of the cracked turbine disc using fracture mechanics principles. In this regard, the fracture mechanics parameters K_I, K_{II}, and K_{III} are calculated, and the corresponding results are presented in the form of graphs, numerical tables, and analytical evaluations. Using these parameters, the stress field in the crack-tip region is examined and the crack growth behavior is analyzed based on the governing fracture mechanics relations. Finally, by applying crack growth models, the remaining life of the turbine disc is estimated [15, 16].

The results obtained from this study can contribute to a better understanding of crack behavior in steam turbine discs and provide useful information for safety assessment, inspection planning, and maintenance strategies in steam power plants [17].

Despite extensive research on the structural integrity and fatigue behavior of steam-turbine discs, several aspects of their fracture and remaining-life assessment remain insufficiently addressed. Previous studies have predominantly focused on conventional fatigue damage, mode-I fracture behavior, or mechanical loading conditions considered independently, while the combined influence of thermal stresses and mechanical loading on mixed-mode crack propagation has received comparatively limited attention. Moreover, fracture assessment and remaining-life prediction have often been treated as separate analyses rather than as an integrated framework.

Figure 3: Sample image of the steam power plant turbine that was studied in this research.

To address these limitations, the present study develops an integrated mixed-mode fracture-mechanics and crack-growth framework for the remaining-life assessment of steam-turbine discs subjected to combined thermal stresses and mechanical loading. The proposed approach considers the interaction of thermal and mechanical stresses, evaluates mixed-mode crack behavior and propagation, and subsequently relates the predicted crack-growth response to the remaining service life of the disc. The main novelty of this work therefore lies in integrating mixed-mode fracture analysis, crack-growth assessment, and remaining-life prediction under combined thermomechanical loading within a unified framework specifically applied to steam-turbine disc components. This approach provides a more comprehensive basis for evaluating structural integrity and supporting life-management decisions for turbine discs operating under complex service conditions.

MATERIAL AND METHOD

The material used for the turbine studied in this research is a heat-resistant martensitic steel of the 12Cr type. Table **1** shows the chemical composition of this alloy, which is widely employed in high-stress and high-temperature components of steam turbines, including blades and rotors. The approximately 12% chromium content imparts thermal stability, oxidation resistance, and enhanced strength at elevated operating temperatures. Following quenching and tempering processes, this steel forms a tempered martensitic structure, providing a combination of high strength, adequate toughness, and desirable creep resistance [18, 19].

The chemical composition of the sample used aligns with typical values for 12Cr steels and is as follows (values may vary slightly depending on the standard and the actual heat):

Table 1: Chemical composition of the 12Cr alloy (wt.%)

Alloy Composition Standard					
Cr: 11–12%	Mo: 0.5–1%	C: 0.10–0.20%	Mn: ≤1%	Si: ≤0.5%	Ni: ≤0.3%

Microalloying elements such as V, Nb, and Ni are added to improve carbide stability and thermal resistance

This composition leads to the formation of stable carbides and a strengthened martensitic microstructure, which is ideal for performance under power plant conditions.

MECHANICAL PROPERTIES AND FRACTURE

12Cr steel exhibits the following key mechanical properties:

- Tensile Strength: Approximately 600–900 Mpa.
- Tensile temperature test: Ambient temperature.
- No special heat treatment.
- Hardness after Tempering: Medium to high, coupled with adequate ductility
- Creep Resistance: Very favorable at temperatures of 500–600°C.
- Fracture Toughness (KIC): In the range of 100 MPa√m, indicating high resistance to crack propagation and sudden fracture.

An initial temperature range of 25–700 °C was considered to establish the thermal boundary conditions, while the resulting temperature field in the critical blade-attachment region was approximately 530–537 °C, which is consistent with the representative high-pressure steam temperature of approximately 540 °C.

These characteristics have made 12Cr steel one of the most commonly used materials in critical steam turbine components, ensuring its behavior under combined mechanical and thermal loading is reliably stable and predictable [19, 20].

MODEL

A standard geometric model (as can be find in Figure **4**), consistent with the actual configuration of the turbine disc investigated in this study and used in steam and combined cycle power plants, was developed. The three-dimensional model of the turbine disc was designed and created using Solid Works software and subsequently used for the numerical analyses in this research.

Figure 4: Three-dimensional model of the turbine disc designed in Solid Works in this research.

ANALYSIS

As can be find in Figure **5**, for maximum accuracy and simulation, both mechanical and thermal modules were employed. The operating temperature conditions of the turbine were applied, and the resulting gradient was applied to the mechanical analysis.

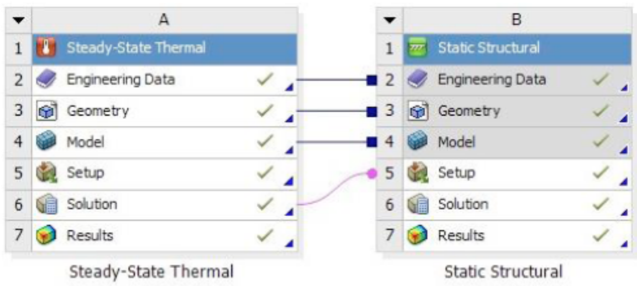

Figure 5: Combined analysis modules used in the present study.

STEADY-STATE THERMAL ANALYSIS

Figures **6** and **7** show the applied temperature gradient. Temperature was between Min 25 and Max 700 ◦C. In this section, to obtain the temperature field of the turbine disc and the temperature gradients (which directly affect thermal stresses and, consequently, the driving force for crack growth), a thermal analysis is performed in the Steady-State Thermal module. The model includes conduction within the disc/blade attachment region, as well as convection heat transfer boundary conditions on surfaces in contact with the steam. In steam power plant turbines, the inlet steam temperature for the high-pressure stage is typically reported around 540°C for common cycles.

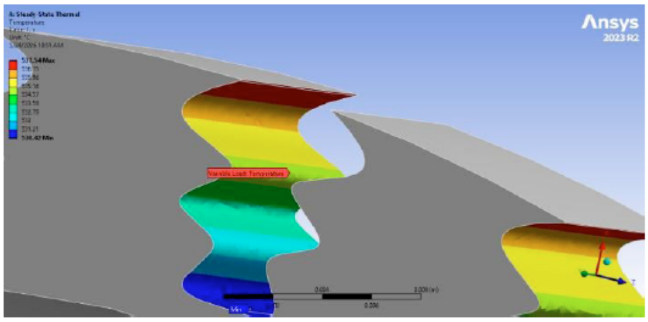

Figure 6: Applied temperature gradient at the junction between the turbine disc and the blade.

In this analysis, heat transfer within the component is modeled through thermal conduction in the solid material and convection boundary conditions applied on the surfaces exposed to the steam flow. A spatially varying temperature load is applied to represent the thermal conditions experienced by the blade root region during turbine operation. The maximum temperature occurs near the upper region exposed to the hot steam, while the temperature gradually decreases toward the lower sections due to heat conduction through the material. The results indicate a temperature range of approximately 530°C to 537°C, forming a thermal gradient along the blade attachment area, which plays an important role in the development of thermal stresses in the structure [21, 22].

Therefore, the boundary conditions were selected to be close to the standard operating conditions of a steam turbine. The material properties of the disc were also considered as an average within the operating temperature range, consistent with martensitic steels/stainless steels commonly used in turbine components (*e.g.*, thermal conductivity of approximately k ≈ 25 W/m·K and specific heat of approximately Cp ≈ 450–500 J/kg·K).

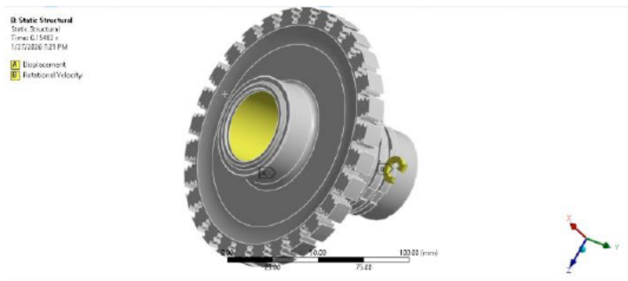

Figure 7: Applied thermal conditions for accurate simulation of the turbine operating environment.

MATERIAL-PROPERTY ASSUMPTIONS AND TEMPERATURE DEPENDENCE

In the present analysis, the 12Cr martensitic steel was modeled as a homogeneous and isotropic material. Although the prescribed thermal boundary range was 25–700°C, the calculated temperature field in the critical blade-attachment region was concentrated within approximately 530–537°C. For the steady-state thermal analysis, representative average values of thermal conductivity (k≈25 W/m·K) and specific heat capacity (Cp≈450–500 J/kg·K) were therefore used to represent the thermal behavior of the material over the considered operating condition.

The mechanical response was evaluated using the mechanical properties defined in the structural model without explicitly incorporating temperature-dependent degradation of elastic or strength properties. Consequently, the present model does not explicitly account for the temperature dependence of elastic modulus, yield strength, plasticity, or creep behavior. This assumption provides a simplified steady-state thermo-mechanical assessment of crack severity under the considered operating condition. The effects of temperature-dependent mechanical properties, creep, and transient thermal loading, particularly during turbine start-up and shutdown, are considered important topics for future investigation.

MECHANICAL ANALYSIS (STATIC STRUCTURAL) - BOUNDARY CONDITIONS AND LOAD APPLICATION

Following the Steady-State Thermal analysis and the determination of the temperature field, the mechanical analysis of the turbine disc is performed in the Static Structural module. This step aims to simultaneously calculate stresses arising from rotation (centrifugal force) and thermal stresses. The primary objective of this phase is to extract the stress/strain field (particularly in critical areas such as the blade root, fillet radius, holes, and hub region) as the basis for crack modeling and the assessment of its growth.

1.1. Transferring the Temperature Field from Thermal Analysis (Thermal Load)

Initially, the results from the thermal analysis are linked to the structural analysis. In Workbench, the Static Structural system is connected to the Steady-State Thermal system (Data Transfer). Within the Mechanical environment, the “Imported Temperature” option is selected under “Loads” to incorporate the actual temperature gradient (not a uniform temperature) into the analysis.

This process naturally yields the thermal stresses according to the following relationship:

$$\sigma_{th} = E\alpha\Delta T \quad (1)$$

1.2. Applying Angular Velocity/Rotation (Rotational Velocity) To simulate the effect of rotor rotation

From the "Loads" section, the "Rotational Velocity" option is selected and applied to the disc body. The axis of rotation is defined along the central axis of the model, corresponding to the shaft axis. A rotational speed of 3000 rpm was selected to represent the operating condition of a 50-Hz steam-turbine generator, corresponding to the synchronous rotational speed commonly adopted for this configuration.

The rotational load induces hoop/radial stresses, which typically intensify in peripheral areas and at locations of geometric discontinuities (Figure **8**).

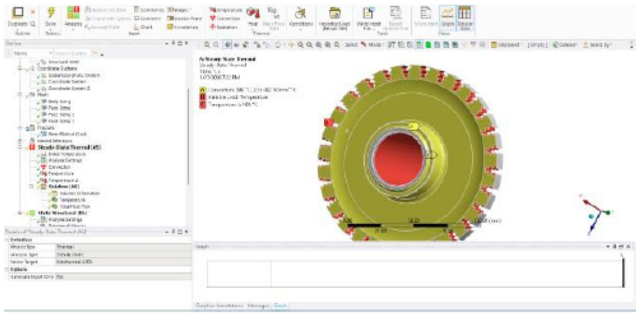

Figure 8: Application of mechanical loading conditions on the turbine disc to accurately simulate the turbine’s mechanical operating conditions.

1.3. Support and Constraints (Fixed Support)

A Fixed Support is applied to the internal surface of the hub/shaft seating area (Bore or Hub Contact Face).

MESHING AND REFINEMENT OF SENSITIVE AREAS

Following the definition of the geometry and application of the boundary conditions, a three-dimensional tetrahedral mesh was generated. Particular attention was given to mesh refinement in regions expected to exhibit high stress and temperature gradients, as well as in geometrically complex regions relevant to crack initiation and propagation. Local Sizing controls were therefore applied to critical regions, including the blade attachment locations, blade roots, fillets, grooves, sharp corners, and other abrupt geometric transitions. Finer elements were employed in these regions, while relatively coarser elements were used in less sensitive regions to maintain a reasonable balance between numerical accuracy and computational cost.

The mesh transition from locally refined regions to the coarser global mesh was controlled using the Transition and Smoothing parameters to avoid abrupt changes in element size and to maintain acceptable mesh quality. Particular attention was given to the regions associated with crack modeling, where local refinement was employed to provide an adequate spatial resolution for the fracture-mechanics calculations.

The quality of the generated mesh was assessed using the Skewness and Element Quality metrics, as illustrated in Figure **9**. Elements exhibiting undesirable quality characteristics in sensitive regions were re-optimized where necessary. The adopted mesh therefore combines local refinement in critical regions with a controlled global element distribution. Although a formal multi-level mesh-convergence analysis was not performed, the adopted local-refinement strategy and mesh-quality assessment were used to improve the numerical reliability of the calculated stress and fracture parameters [23].

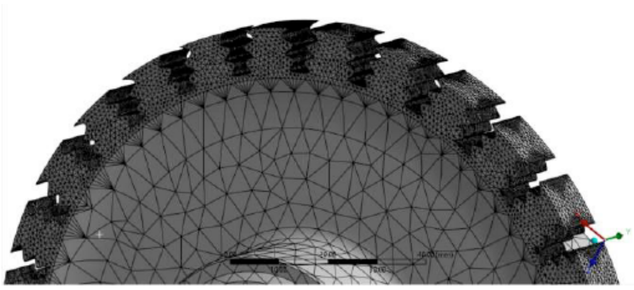

Figure 9: Finite element mesh applied to the turbine disc.

ELEMENT TYPE INFORMATION

Figure **10** shows the element type of solid187. In this numerical modeling, to simulate the three-dimensional behavior of the turbine disk and enable stress analysis and fracture mechanics, second-order volumetric elements have been utilized. As observed in the "Material and Element Type Information" section, the entire model domain has been meshed using SOLID187 elements. This element type is a ten-node tetrahedral element (TET10) and is capable of accurately modeling complex geometries, severe stress and strain gradients, as well as stress concentration zones around cracks.

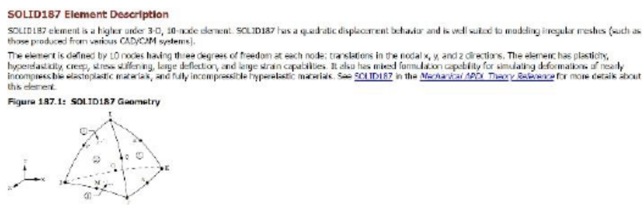

Figure 10: Element type and information of the SOLID187 element used in the finite element model.

In total, 494,134 elements have been defined for the model, indicating a fine mesh and appropriate analysis accuracy, especially in sensitive areas like the blade attachment locations and around the semi-elliptical crack. All elements have been assigned to a single material (Material ID = 1), signifying the uniformity of the turbine disk's mechanical and thermal properties throughout the model. The use of SOLID187 elements, due to their high capability in nonlinear, thermo-mechanical analyses, and fracture mechanics-related problems, is considered a suitable choice for examining stresses and calculating fracture parameters such as the stress intensity factor in this project. Also, the Element information of ANSYS software can be found in Figure **11**.

Material IDs	Element Name IDs	Element Type IDs	Number of Elements
MAT 1	SOLID187	1	494134

Element Name IDs	Material IDs	Element Type IDs	Number of Elements
SOLID187	1	1	494134

Element Type IDs	Element Shape	Material IDs	Element Name IDs	Number of Elements
ETYPE 1	TET10	1	SOLID187	494134

Figure 11: Element information window in ANSYS Mechanical showing the element type and the total number of elements used in the model.

MODELING AND FRACTURE GROWTH WITH MODEL DATA

In this stage, after performing the thermal analysis and transferring the temperature gradient to the mechanical analysis (Static Structural), as well as applying the rotational speed of the disk, the Fracture tool within the Mechanical environment was used to investigate failure behavior and predict crack growth. The initial crack was defined as a Semi-Elliptical Crack located in the critical region near the edge/blade attachment area. It should be noted that the geometric dimensions and orientations of the crack were obtained from real inspection data of the steam power plant turbine disk under study. This was done to examine the effect of stress concentration resulting from rotational and thermal stresses on the increase in crack length.

SENSITIVITY OF THE FRACTURE ASSESSMENT TO MODELING PARAMETERS

The present analysis was performed using a semi-elliptical surface crack with dimensions of 4 mm × 2 mm, a crack orientation of 45°, a thermal boundary range of 25–700°C, and a rotational speed of 3000 rpm. These parameters were selected to represent the investigated turbine-disk configuration and the considered operating condition.

A systematic parametric sensitivity analysis involving variations in crack dimensions, crack orientation, thermal gradient, and rotational speed was not included in the present computational study. Therefore, the reported stress-intensity factors and fatigue-life estimates should be interpreted with respect to the specified reference configuration rather than as universally applicable values. A comprehensive sensitivity analysis covering these parameters would provide further insight into the robustness of the fracture assessment and is identified as an important direction for future work.

EXTRACTION OF STRESS-INTENSITY FACTORS

The Mode I, Mode II, and Mode III stress-intensity factors (KI, KII, and KIII) were extracted using the contour integral approach available in the Fracture tool of ANSYS Mechanical. After defining the semi-elliptical crack, the crack front was discretized into 20 divisions to enable the evaluation of the fracture parameters at different locations along the crack front. Multiple contours surrounding the crack front were considered for the evaluation of the stress-intensity factors. The stress-intensity factors corresponding to the three fracture modes were obtained from the contour-integral calculation and evaluated along the crack front. Because the innermost contour can be more sensitive to local mesh effects and numerical errors, the results from different contours were compared. Contour 3 was selected as the representative contour because it provided stable values with reduced sensitivity to the local numerical effects near the crack tip. The extracted KI, KII, and KIII values were subsequently used to characterize the mixed-mode fracture behavior of the turbine disk.

CRACK DEFINITION ACCORDING TO MODEL SETTINGS

1. Crack Specifications:

- Crack Shape: Semi-Elliptical
- Major Radius (a): 4 mm
- Minor Radius (c): 2 mm

2. Placement and Orientation:

- Coordinate System: Coordinate System 2, a coordinate system oriented at 45° near the blade edge, where dominant cracks are typically initiated and observed due to the applied stresses.
- Align with Face Normal: Yes, the crack orientation is set to align with the normal of the selected surface, ensuring that the crack plane lies precisely on the surface.
- • Crack Front Divisions: 20, the crack front is divided into 20 segments to accurately extract K-values along the crack front.
- • Largest Contour Radius: 0.5 mm, the contour integral radius for calculating K near the crack tip is set to 0.5 mm, which is a reasonable and stable value for millimeter-scale cracks.
- Figure **12** shows the Modeled Crack in ANSYS software.

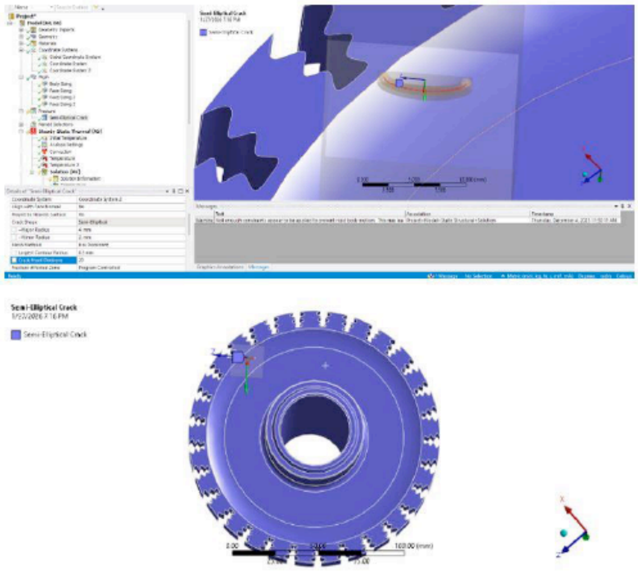

Figure 12: Modeled crack in ANSYS and its application to the turbine disk based on the geometry and dimensions extracted from the real inspected specimen.

RESULTS

Based on the results and as can be find in Figure **13**, the thermo-mechanical and fracture behavior of a steam turbine disk was investigated using Finite Element Analysis (FEA). Initially, a steady-state thermal analysis was performed, yielding a non-uniform temperature distribution across the disk. This indicated a significant thermal gradient between different regions of the disk, particularly near the blade attachment areas. This thermal gradient was then transferred as thermal loading to the mechanical analysis, incorporating the effects of thermal stresses alongside stresses induced by the disk's rotation.

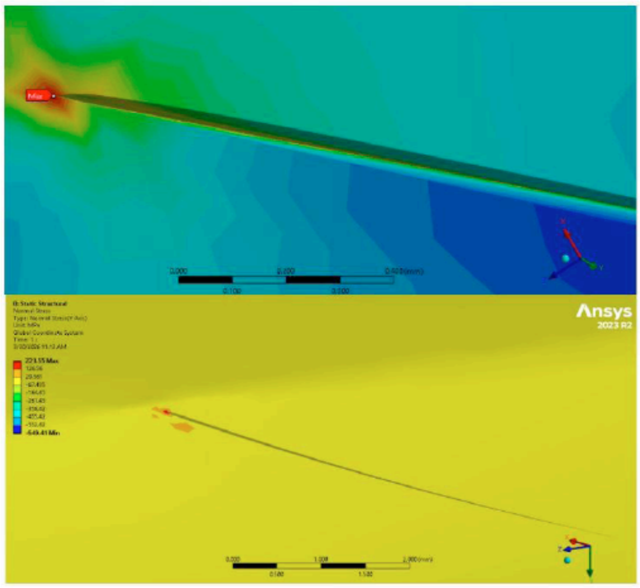

Figure 13: Analysis result showing the normal stress distribution on the crack surface.

The figure above illustrates the results of the finite element analysis conducted in ANSYS software, examining the distribution of normal stress along the Y-axis in the cracked region. Based on the displayed color map, the stress ranges in this analysis vary from a minimum of approximately -649.41 MPa to a maximum of 223.55 MPa.

As observed in the figure, a significant stress concentration is created near the crack tip, where the maximum tensile stress is noted. This stress value is around 223.55 MPa, resulting from the stress concentration phenomenon around the crack tip. As the distance from the crack tip increases, the stress field gradually diminishes, reaching nearly uniform values in other areas of the component. Additionally, some regions adjacent to the crack exhibit considerable compressive stresses, attributed to the stress field distribution and the model's boundary conditions.

The value of the stress perpendicular to the crack, obtained from the finite element analysis results, will be subsequently used to calculate the Stress Intensity Factor (K_I). After determining the stress intensity factor, its range of variation (ΔK) will be utilized in crack growth relationships, such as the Paris' Law: da/dN = C(ΔK)^m, where da/dN represents the crack growth rate per loading cycle. Employing this equation along with the stress field values derived at the crack tip enables the prediction of the crack growth rate and, consequently, the estimation of the component's remaining life. Therefore, the results presented in this figure will serve as the basis for subsequent calculations related to crack growth and remaining life approximation in the following stages of the analysis. Figure **14** shows the crack condition.

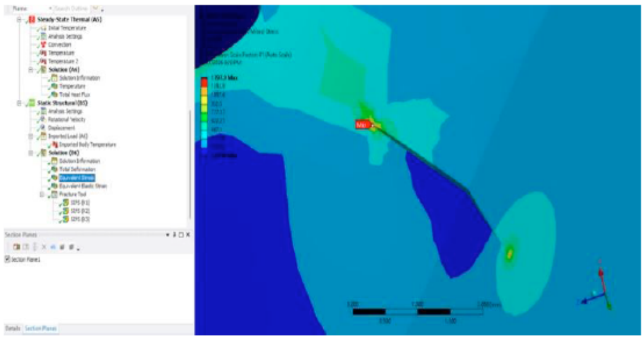

Figure 14: Crack condition and the von Mises stress distribution around the crack region.

FRACTURE MECHANICS PARAMETERS

Fracture mechanics is based on a set of fundamental equations in solid mechanics for analyzing crack behavior in engineering components. These equations include equilibrium equations, compatibility equations, and material constitutive equations.

3D Equilibrium Equations:

$$\frac{\partial \sigma_{xx}}{\partial x} + \frac{\partial \sigma_{xy}}{\partial y} + \frac{\partial \sigma_{xz}}{\partial z} + b_x = 0 \quad (2)$$

$$\frac{\partial \sigma_{yx}}{\partial x} + \frac{\partial \sigma_{yy}}{\partial y} + \frac{\partial \sigma_{yz}}{\partial z} + b_y = 0 \quad (3)$$

$$\frac{\partial \sigma_{zx}}{\partial x} + \frac{\partial \sigma_{zy}}{\partial y} + \frac{\partial \sigma_{zz}}{\partial z} + b_z = 0 \quad (4)$$

Where:

- σ_{ij} represents the stress components.
- b_x, b_y, b_z are the body forces in the coordinate directions

Strain Compatibility Equations in 3D:

The compatibility equations ensure that the strain field resulting from the deformation of the body is continuous and originates from a real displacement field. The 3D compatibility relations are expressed as follows:

$$\frac{\partial^2 \varepsilon_{xx}}{\partial y^2} + \frac{\partial^2 \varepsilon_{yy}}{\partial x^2} = 2\frac{\partial^2 \varepsilon_{xy}}{\partial x\,\partial y} \quad (5)$$

$$\frac{\partial^2 \varepsilon_{yy}}{\partial z^2} + \frac{\partial^2 \varepsilon_{zz}}{\partial y^2} = 2\frac{\partial^2 \varepsilon_{yz}}{\partial y\,\partial z} \quad (6)$$

$$\frac{\partial^2 \varepsilon_{zz}}{\partial x^2} + \frac{\partial^2 \varepsilon_{xx}}{\partial z^2} = 2\frac{\partial^2 \varepsilon_{zx}}{\partial x\,\partial z} \quad (7)$$

$$\frac{\partial^2 \varepsilon_{xy}}{\partial z^2} = \frac{\partial^2 \varepsilon_{yz}}{\partial x\,\partial y} + \frac{\partial^2 \varepsilon_{zx}}{\partial x\,\partial y} - \frac{\partial^2 \varepsilon_{xx}}{\partial y\,\partial z} \quad (8)$$

$$\frac{\partial^2 \varepsilon_{yz}}{\partial x^2} = \frac{\partial^2 \varepsilon_{zx}}{\partial y\,\partial z} + \frac{\partial^2 \varepsilon_{xy}}{\partial y\,\partial z} - \frac{\partial^2 \varepsilon_{yy}}{\partial x\,\partial z} \quad (9)$$

$$\frac{\partial^2 \varepsilon_{zx}}{\partial y^2} = \frac{\partial^2 \varepsilon_{xy}}{\partial x\,\partial z} + \frac{\partial^2 \varepsilon_{yz}}{\partial x\,\partial z} - \frac{\partial^2 \varepsilon_{zz}}{\partial x\,\partial y} \quad (10)$$

These relations state that the strain field must be consistent with a continuous displacement field [24].

Constitutive Equations (3D Hooke's Law):

The constitutive equations define the relationship between stress and strain for the material. For a homogeneous and isotropic linear elastic material, the stress-strain relationships are written as follows:

$$\sigma_{xx} = \lambda(\varepsilon_{xx} + \varepsilon_{yy} + \varepsilon_{zz}) + 2\mu\varepsilon_{xx} \quad (11)$$

$$\sigma_{yy} = \lambda(\varepsilon_{xx} + \varepsilon_{yy} + \varepsilon_{zz}) + 2\mu\varepsilon_{yy} \quad (12)$$

$$\sigma_{zz} = \lambda(\varepsilon_{xx} + \varepsilon_{yy} + \varepsilon_{zz}) + 2\mu\varepsilon_{zz} \quad (13)$$

$$\sigma_{xy} = 2\mu\varepsilon_{xy} \quad (14)$$

$$\sigma_{yz} = 2\mu\varepsilon_{yz} \quad (15)$$

$$\sigma_{zx} = 2\mu\varepsilon_{zx} \quad (16)$$

Where:

$$\mu = \frac{E}{2(1+\nu)} \quad (17)$$

$$\lambda = \frac{\nu}{(1+\nu)(1-2\nu)} \quad (18)$$

And in these relations:

- E is the Young's modulus
- ν is the Poisson's ratio
- λ and μ are Lamé's parameters.

These equations simultaneously describe the stress and strain behavior in a cracked body.

The equilibrium equations express the balance of forces at every point in the body and determine the stress distribution within the material. Alongside these, the compatibility equations ensure that the strain field resulting from the material's deformation is continuous and physically plausible, derived from a valid displacement field. Furthermore, the constitutive equations, based on Hooke's Law for elastic materials, specify the relationship between stress and strain, enabling the calculation of the material's mechanical response under loading.

3D DISPLACEMENT FIELD IN ELASTICITY

Figure **15** shows the behavior of different fracture models. The deformation of a body is described using a displacement vector field. This field relates the location of each point from its initial (unstressed and unstrained) form to its deformed shape. The 3D displacement field is defined as:

$$\mathbf{u}(x,y,z) = \begin{bmatrix} u_x(x,y,z) \\ u_y(x,y,z) \\ u_z(x,y,z) \end{bmatrix} \quad (19)$$

where u_x , u_y , and u_z are the displacement components in the x, y, and z coordinate directions, respectively. This field adds three independent unknowns to the system of elasticity equations.

By simultaneously solving these equations, the stress and strain fields around the crack can be calculated. In linear elastic fracture mechanics, the behavior of the stress field near the crack tip is described by a parameter called the Stress Intensity Factor (SIF), denoted by the symbol K. This parameter represents the intensity of stress concentration in the vicinity of the crack tip and depends on factors such as the geometry of the component, the crack length, and the type of loading. Based on this analysis, three primary modes of fracture are defined: Opening Mode (Mode I), In-plane Shear Mode (Mode II), and Out-of-plane Shear Mode (Mode III), which are characterized by the stress intensity factors K_I, K_{II}, and K_{III}, respectively.

In polar coordinates (r,θ) with the origin at the crack tip, the stress field is expressed as:

$$\sigma_{ij}(r,\theta) = \frac{K}{\sqrt{2\pi r}} f_{ij}(\theta) \quad (20)$$

where:

- K is the Stress Intensity Factor
- r is the distance from the crack tip
- θ is the angle with respect to the crack plane
- $f_{ij}(\theta)$ are angular functions dependent on the type of loading mode.

This relationship indicates that the stress near the crack tip exhibits a singularity behavior of the order $1/\sqrt{r}$ [25].

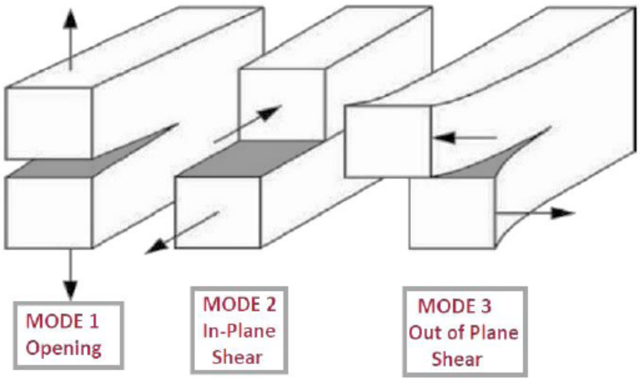

Figure 15: The behavior of each fracture mode.

As can be find in Figures **16**, Figure **17** and Figure **18**, the dominant fracture mode is Mode II. The maximum Mode I stress intensity factor along the crack front is the following value.

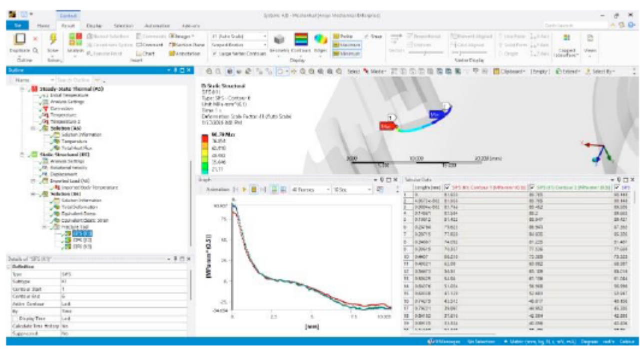

Figure 16: Mode I stress in the component and K1 values.

While the values of Modes I and III are smaller in comparison and therefore play a secondary role in the fracture behavior, these results indicate that the primary mechanism of crack propagation in the turbine disk is the in-plane shear sliding of the crack under the influence of effective tensile stresses generated by rotational loading and thermal stresses.

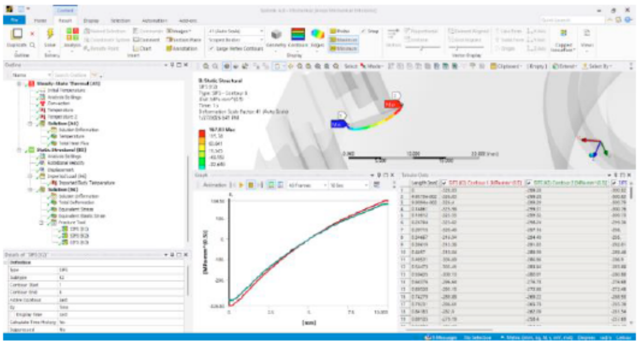

Figure 17: Mode II stress in the component and K2 values.

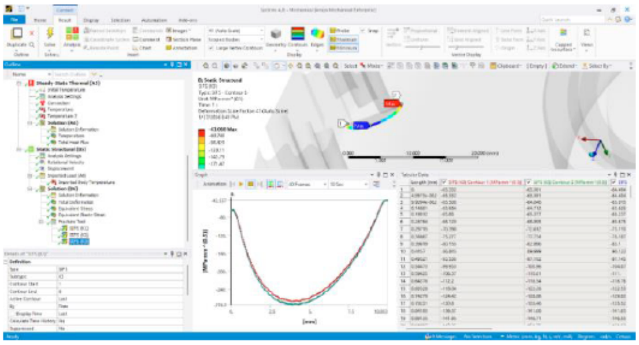

Figure 18: Mode III stress in the component and K3 values.

In the calculation of the stress intensity factor (Figure **19**), the values of $K$are extracted from several contours surrounding the crack tip. The initial contours (such as Contour 1), due to their strong dependence on mesh refinement and numerical effects near the crack tip, usually exhibit greater fluctuations and higher numerical errors. In contrast, contours located farther away may deviate from the singular stress field region. Accordingly, the third contour (Contour 3) was selected as an intermediate contour, since it provides a suitable balance between numerical accuracy and result stability. The proper convergence of the stress intensity factor values in this contour indicates that the obtained results are mesh-independent and possess acceptable numerical reliability.

$K_{I,\max} \approx 90.148\ \mathrm{MPa}\sqrt{\mathrm{mm}}$

$K_{II,\max} \approx 167.93\ \mathrm{MPa}\sqrt{\mathrm{mm}}$

$K_{III,\max} \approx 64.404\ \mathrm{MPa}\sqrt{\mathrm{mm}}$

The calculation of stress intensity factors enables the evaluation of crack growth conditions and the prediction of fracture behavior in engineering components. In general, if the value of the stress intensity factor reaches the critical value of the material, known as K_{IC}, the crack will propagate unstably and

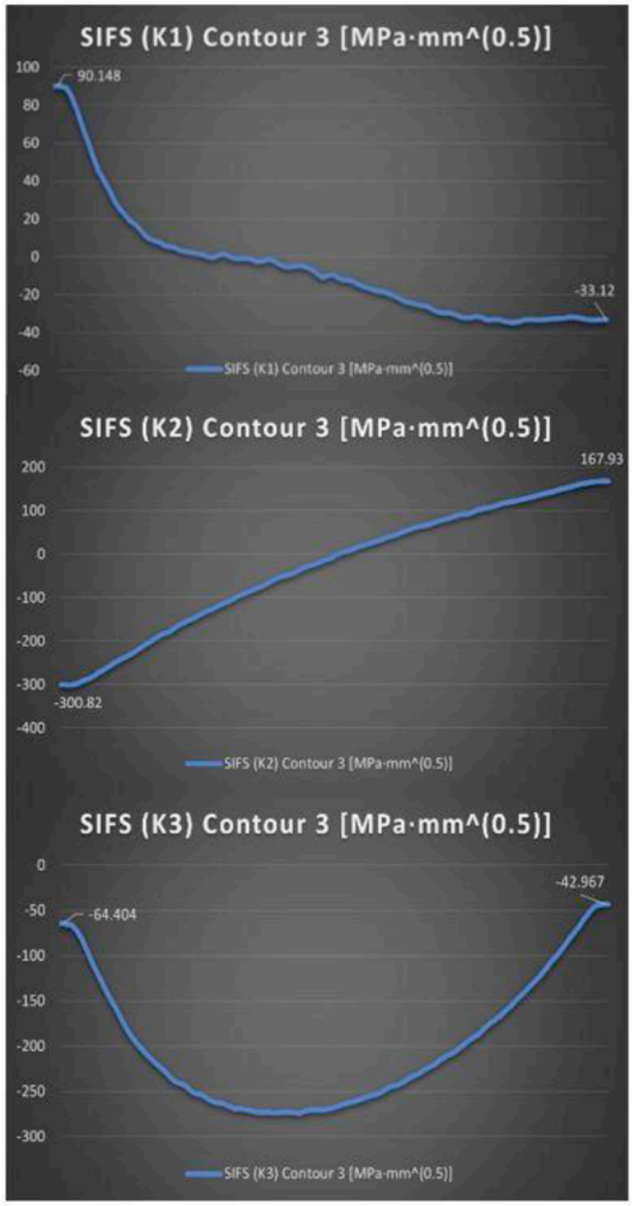

Figure 19: SIFs (K_1, K_2, K_3) – Contour 3 Diagram.

fracture will occur. Therefore, the application of fracture mechanics equations and the calculation of the parameter K play a fundamental role in structural safety analysis, prediction of the remaining service life of components, and prevention of sudden failures in equipment such as steam turbine disks. Fracture occurs when the stress intensity factor reaches the critical value of the material:

$$K_{eff} = K_{IC} \quad (21)$$

where K_{IC} represents the fracture toughness of the material.

CALCULATION OF THE EFFECTIVE STRESS INTENSITY FACTOR (MIXED MODE)

Under mixed-mode loading conditions, the onset of fracture depends on the vector combination of the modes and can be evaluated using the following criterion [26]:

$$K_{eff} = \sqrt{K_I^2 + K_{II}^2 + K_{III}^2} \quad (22)$$

Substituting the numerical values:

$$K_{eff} = \sqrt{(2.85)^2 + (5.31)^2 + (2.04)^2}$$

$$K_{eff} = \sqrt{40.48} = 6.36 \text{ MPa}\sqrt{m}$$

COMPARISON WITH THE FRACTURE TOUGHNESS OF 12CR STEEL

12Cr steels (martensitic steels containing approximately 12% chromium) constitute an important class of heat-resistant steels that are widely used in high-temperature and high-pressure equipment such as thermal power plants, boilers, turbines, and steam pipelines. Owing to their specific alloying composition, these steels exhibit very favorable mechanical behavior under elevated temperatures and corrosive environments.

The fracture toughness of this steel is approximately:

$$K_{IC} \approx 100 \text{ MPa}\sqrt{m}$$

Considering that:

$$K_{eff} = 6.36 \text{ MPa}\sqrt{m} \ll K_{IC}$$

The effective stress intensity factor is significantly lower than the critical fracture limit. However, this does not imply the complete elimination of risk. Rather, the potential future crack growth behavior must be predicted, periodic inspection programs should be established accordingly, and, most importantly, the remaining life of the component must be carefully evaluated.

EVALUATION OF THE REMAINING LIFE OF THE COMPONENT

In order to estimate the remaining life of the component, a fatigue crack growth analysis was performed based on the principles of fracture mechanics. Within this framework, one of the key steps in life assessment is the consideration of safety factors in the evaluation of fracture parameters. The application of a safety factor directly affects the critical crack size (a_c)and consequently limits the allowable range of crack growth.

In this study, the effect of the safety factor was considered by applying a factor of 2 to the fracture toughness of the material. This approach effectively reduces the effective fracture toughness value and consequently decreases the acceptable critical crack size. Reducing the critical crack size ensures that the crack is detected and controlled before reaching larger dimensions, thereby increasing the safety level of the analysis.

FATIGUE CRACK GROWTH MODEL

To model the gradual growth of the crack from the initial crack size to the modified critical crack size, the Paris law was employed [27]. The Paris law provides an established empirical relationship between the fatigue crack-growth rate and the stress-intensity-factor range in the stable crack-growth regime:

$$\frac{da}{dN} = C(\Delta K)^m \quad (23)$$

Where da/dN represents the crack-growth rate per loading cycle, ΔK is the stress-intensity-factor range, and C and m are the Paris-law model parameters. In the present study, $C=10^{-12}$ and m=3 were adopted as representative model parameters based on engineering experience and preliminary trial-and-error assessment to obtain a physically reasonable fatigue crack-growth response. These parameters were not independently calibrated against experimental fatigue crack-growth data for the investigated material. Therefore, the Paris-law analysis is used here as a model-based fatigue-life estimation rather than as an experimentally calibrated prediction of material-specific crack-growth behavior (Of course, it is noteworthy that the selection of the values of C and m was not based solely on experience, and similar numbers are mentioned in some references [28]).

$C = 1\times10^{-12}$

$m = 3$

$Y = 1.1$

$\sigma = 223.55$ MPa

$a_0 = 4$ mm

a_c: critical crack size considering the safety factor

The fatigue stress intensity factor range is calculated as:

$$\Delta K = Y\sigma\sqrt{\pi a} \quad (24)$$

The critical crack size considering a safety factor of 2 is approximately:

$$a_c \approx 13 \text{ mm}$$

FATIGUE LIFE CALCULATION

By substituting the expression for ΔKinto the Paris law and integrating from the initial crack size to the modified critical crack size, the fatigue life of the component can be obtained as:

$$N = \frac{1}{C(Y\sigma)^3\pi^{3/2}}\left(\frac{1}{\sqrt{a_0}} - \frac{1}{\sqrt{a_c}}\right) \quad (25)$$

In this relation, the initial crack size a_0 has a fixed value, while the value of a_c is directly influenced by the applied safety factor. Therefore, any change in the critical crack size can directly affect the predicted fatigue life of the component.

ANALYSIS OF THE EFFECT OF THE SAFETY FACTOR ON COMPONENT LIFE

Increasing the safety factor leads to a reduction in the critical crack size. However, it should be noted that in many engineering components, a significant portion of the fatigue life is consumed during the early stages of crack growth, particularly within the slow crack growth region. In the present study, it was also observed that the largest contribution to the total life corresponds to crack growth from approximately 4 mm to about 8–9 mm.

Therefore, although reducing the critical crack size decreases the final allowable crack growth range, its effect on the total predicted fatigue life is relatively limited.

Nevertheless, the application of a safety factor is of great importance from the perspectives of structural safety and reliability, since it prevents the crack from reaching sizes that significantly increase the likelihood of sudden failure.

FATIGUE LIFE CALCULATION RESULT

Considering the above parameters and applying the safety factor in determining the critical crack size, the fatigue life of the component was estimated as:

$N \approx 1.4\times10^{8}$ cycles

This value represents the number of loading cycles that the component can withstand until the crack reaches the modified critical size under the conditions considered in the present analysis.

CONCLUSION AND RECOMMENDATIONS FOR ENGINEERS

In this study, the fracture behavior of a power plant steam turbine disk subjected to the combined effects of thermal stresses and rotational mechanical loading was investigated based on the principles of fracture mechanics and finite element numerical analysis. The results showed that the presence of a crack in the disk, although it does not lead to immediate unstable fracture under normal operating conditions, cannot be neglected. The presence of such a defect transforms the failure mechanism from a simple uniaxial stress problem into a complex mixed-mode fracture problem.

The analysis of the stress intensity factors extracted from the intermediate contour around the crack tip indicated that:

$K_{II,\max} \approx 167.93\ \text{MPa}\sqrt{\text{mm}}$

is higher than

$K_{I,\max} \approx 90.148\ \text{MPa}\sqrt{\text{mm}}$

and

$K_{III,\max} \approx 64.404\ \text{MPa}\sqrt{\text{mm}}$

Therefore, the dominant crack growth mechanism in the investigated turbine disk is Mode II (in-plane shear), while Modes I and III play secondary but non-negligible roles. This result is consistent with the nature of the combined stresses acting on the turbine disk—namely the tensile stresses induced by rotation and thermal gradients—and highlights that safety assessment of such components cannot rely solely on Mode I fracture analysis. By calculating the effective stress intensity factor

$$K_{eff} = \sqrt{K_I^2 + K_{II}^2 + K_{III}^2} \quad (26)$$

the obtained value:

$K_{eff} = 6.36\ \text{MPa}\sqrt{\text{m}}$

was compared with the fracture toughness of 12Cr steel $\left(K_{IC} \approx 100\ \text{MPa}\sqrt{\text{m}}\right)$. The comparison indicates that, under the studied operating conditions, a significant safety margin exists with respect to unstable fracture. Nevertheless, the relatively low value of K_{eff} compared with K_{IC} does not imply the complete elimination of risk, since fatigue fracture mechanics demonstrates that even relatively low stress intensity factors may cause gradual crack propagation over time until the crack reaches its critical size.

In the next stage, crack growth was modeled using the Paris law while considering the material parameters and loading conditions

$C = 10^{-12}$, $m = 3$, $Y = 1.1$, $\sigma = 223.55$ MPa

The crack propagation from the initial crack size

$a_0 = 4$ mm

to the modified critical crack size

$a_c \approx 13$ mm

(Obtained by applying a safety factor of 2 to the fracture toughness) was simulated. The analysis showed that the majority of the fatigue life is consumed during the slow crack growth phase, particularly when the crack grows from its initial few millimeters to the intermediate crack length region. Increasing the safety factor reduces the allowable critical crack size and consequently decreases the predicted service life; however, from an engineering standpoint this conservative approach is essential to ensure structural safety and reliability. In other words, selecting a conservative value for a_c reduces the allowable operational life but significantly lowers the risk of sudden catastrophic failure.

These findings convey several important engineering implications. First, mixed-mode fracture mechanics analysis is essential for turbine disks, especially in the presence of surface or subsurface cracks, and provides a more reliable framework than conventional allowable stress approaches. Second, the combined use of finite element analysis (FEA) for accurate determination of stress fields and stress intensity factors, together with fatigue crack growth models for remaining life prediction, offers a powerful tool for engineers to design periodic inspection programs, implement condition monitoring strategies, and make informed decisions regarding repair or replacement schedules. Third, the results indicate that the investigated disk is currently in a safe condition with respect to instantaneous fracture; however, continued operation without systematic crack growth monitoring could pose long-term risks.

LIMITATIONS AND UNCERTAINTIES OF THE REMAINING-LIFE PREDICTION

The predicted remaining fatigue life should be interpreted in the context of the assumptions adopted in the present fracture-mechanics model. In particular, uncertainties are associated with the Paris-law parameters C and m, which were selected based on engineering judgment and preliminary sensitivity assessment rather than independently calibrated using experimental fatigue crack-growth data for the investigated material. Consequently, variations in these parameters may affect the predicted crack-growth rate and remaining fatigue life.

Additional uncertainties arise from the assumed loading conditions. The present analysis considers a steady-state thermal field and a rotational speed of 3000 rpm, whereas actual turbine operation may involve variations in rotational speed, thermal gradients, start-up and shutdown cycles, and other transient loading effects. Furthermore, the material was modeled using representative average properties without explicitly accounting for temperature-dependent changes in mechanical properties, creep behavior, or material variability.

Therefore, the reported remaining-life value should be regarded as a model-based quantitative estimate for the specified crack geometry and operating conditions rather than an exact service-life prediction. Incorporating experimentally calibrated crack-growth parameters, temperature-dependent material properties, variable operational loading, and probabilistic treatment of the relevant uncertainties would improve the reliability and conservatism of future remaining-life assessments.

CONCLUSION

This study investigated the mixed-mode fracture behavior and fatigue crack-growth characteristics of a steam turbine disk using a fracture-mechanics-based approach. The principal findings of the study can be summarized as follows:

1. The calculated stress-intensity factors for the investigated crack configuration were K_I=90.148, K_{II}=167.93, and K_{III}=64.404 MPa$\sqrt{mm}$, respectively. After conversion to MPa$\sqrt{m}$, these values correspond to approximately 2.850, 5.310, and 2.037 MPa$\sqrt{m}$, respectively. The results indicate a pronounced mixed-mode loading condition, with Mode II providing the largest contribution to the stress-intensity response.

2. The effective stress-intensity factor was determined as Keff=6.36 MPa$\sqrt{m}$ after unit conversion. This parameter provides a quantitative basis for evaluating the severity of the investigated crack under the considered loading condition and for comparing the crack-driving force with the corresponding fracture-toughness criterion.

3. The fatigue crack-growth behavior was evaluated using the Paris law, with $C=10^{-12}$ and m=3 adopted as model parameters based on engineering judgment and preliminary sensitivity assessment. Since these parameters were not independently calibrated using experimental fatigue crack-growth data for the investigated material, the resulting fatigue-life assessment should be regarded as a model-based quantitative estimate rather than an experimentally calibrated material-specific prediction.

4. The engineering contribution of this study is the development and application of a quantitative fracture-mechanics-based framework for assessing crack severity and fatigue-crack growth in steam turbine disks under mixed-mode loading. The obtained stress-intensity factors and fatigue-life assessment can provide useful support for engineering decisions

regarding crack criticality, inspection planning, maintenance scheduling, and the prevention of unexpected turbine-disk failure.

5. The calculated mixed-mode stress-intensity factors provide quantitative indicators of crack severity in critical regions of the turbine disk and can support fracture-criticality assessment. Combined with the fatigue crack-growth analysis, these results can assist in prioritizing inspection and maintenance actions and in evaluating operational safety under the considered loading conditions. However, the predicted fatigue life should be regarded as a supporting engineering indicator rather than a standalone basis for defining inspection intervals.

Future work should incorporate transient thermal loading associated with frequent start-up and shutdown cycles, microstructural anisotropy, and the statistical variability of fatigue crack-growth parameters. Sensitivity analysis and probabilistic fracture-mechanics approaches can further improve the robustness and conservatism of remaining-life assessments under realistic service conditions.

AUTHOR'S CONTRIBUTION STATEMENT

All authors contributed to the study conception and design. Data collection and analysis were performed by Mohammad Farahi and Amir Mahdi Ebrahimi. 3D model design by Mohammad Farahi. The first draft of the manuscript was written by Arina Agharafiee, and all authors commented on previous versions of the manuscript. All authors read and approved the final manuscript. The project manager was Omid Ashkani"

DATA AVAILABILITY

All data will be provided upon request from the corresponding authors.

COMPETING INTERESTS

The authors declare no relevant financial or non-financial interests.

CONSENT FOR PUBLICATION

All authors read and approved the final manuscript for publication.

ACKNOWLEDGEMENT DECLARATION

Not applicable.

FUNDING DECLARATION

No Funding.

REFERENCES

[1] T. L. Anderson, Fracture Mechanics: Fundamentals and Applications, 4th ed. Boca Raton: CRC Press, 2017. https://doi.org/10.1201/9781315370293

[2] Zerbst, U., Madia, M., Vormwald, M., & Beier, H. Th. (2018). Fatigue strength and fracture mechanics – A general perspective. Engineering Fracture Mechanics, 198, 2-23. https://doi.org/10.1016/j.engfracmech.2017.04.030

[3] Mechanisms of interior crack initiation in very-high-cycle fatigue of highstrength Alloys Xiaolong Liu, Erqing Chen, Fan Zeng, Tao Cong, Joseph P. Domblesky.

[4] Stress-dependent opening- and shear-mode propagation behavior of fatigue cracks in ultrafine-grained Cu fabricated by equal channel angular pressing M. Goto, T. Yamamoto, S.Z. Han, S. Kim, J. Kitamura, T. Yakushiji, J-H. Ahn, R. Takanami, T. Utsunomiya, J. Lee.

[5] D. Broek, Elementary Engineering Fracture Mechanics. The Hague: Martinus Nijhoff Publishers, 1982. https://doi.org/10.1007/978-94-009-4333-9

[6] ductile cast iron based on strain increase tests and evaluation of cyclic deformation behavior in isothermal measuring intervals Benjamin Jost, Marcus Klein, Tilmann Beck, Dietmar Eifler.

[7] Biogas partial oxidation in a heat recirculation reactor for syngas production and CO2 utilization https://doi.org/10.1016/j.apenergy.2018.02.123 Received 1 May 2017; Received in revised form 16 February 2018; Accepted 17 February 2018 ⁎ 0306-2619/ © 2018 Elsevier Ltd. All rights reserved.

[8] Effects of span-depth ratios on the energy release rate for three-point bending beams Received 3 February 2020; Received in revised form 18 January 2021; Accepted 19 January 2021.

[9] Failure Analysis of Steam Turbine Blade Roots He Hua, Zheng Zhunbei, Yang Zhanjun, Xiaochen Wang, Wu Yuxing.

[10] A plastic stress intensity factor approach to turbine disk structural integrity assessment V. Shlyannikov *et al*ii, Frattura ed Integrità Strutturale, 37 (2016) 193-199. https://doi.org/10.3221/IGF-ESIS.37.25

[11] Thermomechanical fatigue crack growth in a single crystal nickel base superalloy Frans Palmert, Johan Moverare, David Gustafsson PII: S0142-1123(19)30026-X.

[12] Fracture mechanics analysis of damaged turbine rotor discs using finite element method by Ivana V. Vasovi]1 Stevan M. Maksimovi]2, Dragi P.STAMENKOVI]3, Slobodan N. STUPAR 4, Mirko S. MAKSIMOVI]5 and Gordana M. BAKI]4.

[13] Review of fracture toughness (G, K, J, CTOD, CTOA) testing and standardization Xian Kui Zhu a James A. Joyce b a Battelle Memorial Institute, 505 King Avenue, Columbus, OH 43201, USA b Mechanical Engineering Department, US Naval Academy, 590 Holloway Road, Annapolis, MD 21402, USA.

[14] The crack growth in the imitation model of a gte turbine disk under operating loading conditions.

[15] Wang, Y., Wang, W., Zhang, B., & Li, C.-Q. (2017). A review on mixed mode fracture of metals. Engineering Fracture Mechanics, 178, 180-206. https://doi.org/10.3901/JME.2017.10.180

[16] Ajdani, A., Ayatollahi, M. R., Akhavan-Safar, A., & da Silva, L. F. M. (2021). Mixed mode fracture characterization of brittle and semi-brittle adhesives using the SCB specimen. International Journal of Adhesion and Adhesives, 109, 102898. https://doi.org/10.1016/j.ijadhadh.2020.102629

[17] Kahlin, M., Ansell, H., & Moverare, J. (2022). Fatigue crack growth for through and part-through cracks in additively manufactured Ti6Al4V. International Journal of Fatigue, 155, 106608. https://doi.org/10.1016/j.ijfatigue.2021.106608

[18] Rotor thermal stress monitoring in steam turbines Bouberle Antonín, Jakl Jan, Liška Jindřich NTIS – New Technologies for the Information Society, University of West Bohemia,

Czech Republic Journal of Physics: Conference Series 659 (2015) 012044. https://doi.org/10.1088/1742-6596/659/1/012044

[19] Effect of aging temperature on the heterogeneous microstructure and mechanical properties of a 12Cr–10Ni–Mo–Ti maraging steel for cryogenic applications Honglin Zhang1,2,3, Mingyue Sun1,3,*, Dongping Ma4, Bin Xu1,3, Taijiang Wang4, Dianzhong Li3, and Yiyi Li3.

[20] Effect of the Thermo-Mechanical Processing on the Impact Toughness of a 12% Cr Martensitic Steel with Co, Cu,W, Moand Ta Doping Alexandra Fedoseeva 1,2 , Ivan Nikitin 1, Nadezhda Dudova 1,* , John Hald 3 and Rustam Kaibyshev 2 Metals 2022, 12, 3. https://doi.org/10.3390/met12010003

[21] Song, H., Xie, K., & Gao, C. (2021). Temperature, thermal flux and thermal stress distribution around an elliptic cavity with temperature-dependent material properties. International Journal of Solids and Structures, 216, 136-144. https://doi.org/10.1016/j.ijsolstr.2021.01.010

[22] Li, D., Yuan, H., Ma, S., & Yang, J. (2022). Dynamic coupling analysis on thermo–chemo–mechanical field and fluid–structure interaction for aero-engine turbine blade with functional gradient thermal barrier coatings. Coatings, 12, 1498. https://doi.org/10.3390/coatings12101498

[23] Zienkiewicz, O. C., & Taylor, R. L. (2013). The finite element method for solid and structural mechanics (6th ed.). Oxford, UK: Elsevier Butterworth-Heinemann.

[24] Irwin, G. R. (1957). Analysis of stresses and strains near the end of a crack traversing a plate. Journal of Applied Mechanics, 24, 361-364. https://doi.org/10.1115/1.4011547

[25] Newman, J. C., Jr., & Raju, I. S. (1981). An empirical stress-intensity factor equation for the surface crack. Engineering Fracture Mechanics, 15(1-2), 185-192. https://doi.org/10.1016/0013-7944(81)90116-8

[26] Zerbst, U., Vormwald, M., Pippan, R., Gänser, H.-P., Sarrazin-Baudoux, C., & Madia, M. (2016). About the fatigue crack propagation threshold of metals as a design criterion – A review. Engineering Fracture Mechanics, 153, 190-243. https://doi.org/10.1016/j.engfracmech.2015.12.002

[27] Paris, P., & Erdogan, F. (1963). A critical analysis of crack propagation laws. Journal of Basic Engineering, 85(4), 528-534. https://doi.org/10.1115/1.3656900

[28] Schönbauer, B. M., & Stanzl-Tschegg, S. E. (2013). Influence of environment on the fatigue crack growth behaviour of 12% Cr steel. Ultrasonics, 53(8), 1399-1405. https://doi.org/10.1016/j.ultras.2013.02.007

https://doi.org/10.31875/2409-9848.2026.13.06